

Preliminary Mission Design and Analysis of a Lunar Far-side Positioning CubeSat Mission

By Hongru CHEN,¹⁾ Lei LIU,²⁾³⁾ Yazhe MENG,¹⁾⁴⁾ Zhenyu XU,¹⁾⁴⁾ Long LONG,¹⁾⁴⁾ and Jiangkai LIU¹⁾⁴⁾

¹⁾Key Laboratory of Space Utilization, Technology and Engineering Center for Space Utilization, Chinese Academy of Sciences, Beijing, China

²⁾College of Science, National University of Defense Technology, Changsha, China

³⁾Beijing Aerospace Control Center, Beijing, China

⁴⁾University of Chinese Academy of Sciences, Beijing, China

The far side of the moon will be explored in the near future. However, challenges of navigation and communication arise as the far side is not visible to the Earth. A mission consists of four CubeSats deployed along an Earth-moon L_2 (EML2) halo orbit to provide the positioning service is proposed. The reasons include that 1) EML2 halo orbits are always visible to the Earth and the moon, and 2) CubeSats are miniature and thus can be carried along with a lunar lander by a mother spacecraft aimed at the Moon. The preliminary mission design and analysis include assessments of the spatial and temporal coverage and accuracy of the positioning service, the trajectory design for deployment and station keeping, and discussions on the system design.

Key Words: Lunar Far Side, Positioning, Constellations, Lunar CubeSats, Trajectory Optimization

1. Introduction

The Martian mission Insight is planned to carry two CubeSats, MarCo, which is to provide the communication relay during Insight landing on Mars.¹⁾ The AIM mission is planned to rendezvous the binary asteroid 65803 Didymos and then deploy a lander and two or more CubeSats to perform inter-satellite network.²⁾ The Exploration Mission 1 has selected 13 CubeSat companions.³⁾ Therefore, it is reasonable to believe CubeSats will play an important role in future interplanetary missions, and the cooperative operation by distributed elements in space is a promising manner. In this context, the present work investigates a mission involving CubeSat deployments to assist the positioning of landers/rovers on the far side of the moon.

There will be missions aimed at the far side of the moon in the near future.⁴⁾ The terrain and resources on the far side of the moon are very different from those on the near side, and hence worth exploring. In addition, the far side is an ideal platform for radio astronomy as the moon can shield the radio noise from the Earth. China will land the Chang'E-4 on the far side in 2018.⁵⁾ However, challenges for navigation and communication arise, as the far side is invisible to the Earth. Moreover, as the terrain on the far side is very rough, the requirement of landing accuracy is even strict. Hill and Born,⁶⁾ and Hesar et al.⁷⁾ have studied the technique of tracking the satellites in an Earth-Moon L_2 (EML2) halo orbit and landers on the far side of the moon using inter-satellite ranging. However, that technique is applicable for non-maneuvering objects. For real-time positioning of maneuvering objects, such as a lander performing pinpoint landing, multiple reference points are required. Similar to the GPS technique, at least four references are necessary. A mission consists of four CubeSats deployed along an Earth-moon L_2 (EML2) halo orbit to provide the positioning service is proposed. The halo orbit is a three-dimensional periodic orbit about a collinear libration point in the three-body system. The EML2 halo orbit can always be seen from the Earth and

the far side of the moon, and therefore is favorable for constant communication as well as tracking.

The preliminary design and analysis presented in this paper include assessments of the spatial and temporal coverage of the lunar surface, accuracy of the positioning service, and the required Δv budget. The Δv budget should cover the needs of deploying the four CubeSats along a halo orbit and the station keeping of the halo orbit, which are presented as well. The optimization of continuous-thrust trajectory is also carried out, result of which serves as a reference for propulsion system sizing.

2. Mission Overview

The dynamics environment of the Earth-moon system can be well approximated by the circular restricted three-body problem (CR3BP). There are five equilibrium points where relative acceleration and velocity to the Earth-moon rotating frame are zero. They are also termed libration points or Lagrangian points labeled as L_1, \dots, L_5 . The halo orbit is a three-dimensional periodic orbit around a collinear point, L_1, L_2 , or L_3 . A halo orbit can be computed using numerical differential correction,⁸⁾ and a family of halo orbits can be computed using pseudo-arc-length continuation method.⁹⁾ Fig. 1 shows the family of EML2 halo orbits in the moon-centered rotating frame. As seen in the figure, the halo orbits can be extended to the vicinity of the moon. This group of orbits are termed near rectilinear halo orbits (NRHO).

The Earth-moon L_2 (EML2) point is 64,500 km from the moon on the far side. The halo orbits around EML2 are visible to both the Earth and the far side of the moon. Moreover, the directions of the lines of sight to the Earth and the Moon are almost aligned, which is favorable for communication as well as attitude control. Therefore, it is desirable to deploy four 6U CubeSats along an EML2 halo orbit to support the positioning of users on the far side of the moon (see Fig. 2).

2.1. System Design

The positions of the CubeSats are determined by processing the ranging data from the ground stations on Earth. With the positions of the CubeSats known, through ranging between the user on the far side of the Moon and the CubeSats, the user can resolve its position through a proper estimation algorithm. The CubeSats are similar to communication relay satellites. The CubeSat system has to be small and simple. For this mission, the payload of the CubeSats are basically the communication system, which is capable of ranging. Due to the limited power of CubeSats, the normal mode of the CubeSats is waiting for commands from the Earth and the moon, which are received via the VHF/UHF antennas at low power consumption. Once the ground stations on the Earth or the lunar users (landers or rovers) are requesting ranging and position data of the CubeSats, the CubeSats will transmit data via the on-board S-band middle-gain and low-gain antennas at a power of 30W. The status information of the lunar lander and the measurement data of the moon can also be sent to the Earth via the CubeSats. According to this concept, components of a CubeSat are decided, which is given in Table 1. The mass of the CubeSat without a propulsion system is around 4.8 kg and the occupied volume is 3 U. A 6U frame is used with a 3U space allocated to the propulsion system, which will be discussed in Sec. 5. The momentum of reaction wheels is unloaded by the reaction control thrust provided by the propulsion system. The layout of the CubeSat is shown in Fig. 3.

3. Positioning Performance

3.1. Positioning Accuracy

The position error (ΔR) of the lunar user can be expressed as the product of the pseudo-range error ($\Delta\rho$) and a geometric index, that is,

$$\Delta R = PDOP \times \Delta\rho \quad (1)$$

where $PDOP$ (Position Dilution of Precision) is related to the geometry of the CubeSats with respect to the user. $PDOP$ can

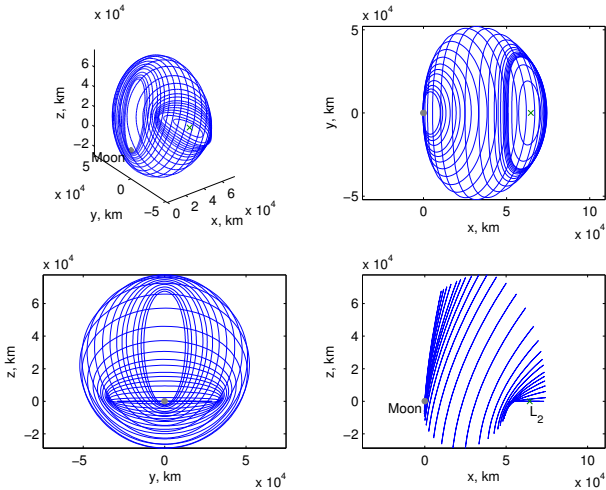


Fig. 1. Earth-moon L_2 halo orbits.

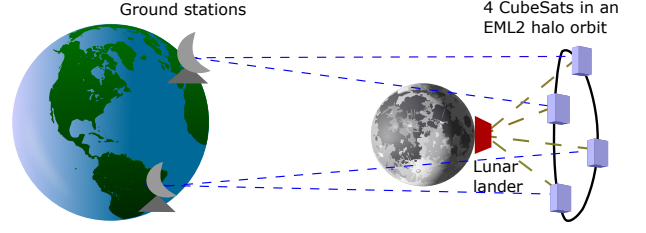


Fig. 2. Schematic of tracking CubeSats and landers on the far side of the moon.

Table 1. Components of the CubeSat (without propulsion system)

Subsystems	Components	mass, g
Structure	1 6U frame	1600
	2 deployable panels	
Power	Solar arrays (33W)	1200
	1 battery (72Whr)	
ADCS	4 Reaction wheels	750
	1 Star Tracker	
	1 MEMS IMU	
	4 Sun sensors	
Communication	4 UHF antennas	700
	3 Low-gain antennas	
	1 Middle-gain antennas	
	1 Radio transponder	
C&DH	OBC	200
Other	Atomic clock	340
Total		4790

be computed from,

$$\mathbf{P} = \begin{bmatrix} \frac{(x_1-x)}{R_1} & \frac{(y_1-y)}{R_1} & \frac{(z_1-z)}{R_1} & -1 \\ \frac{(x_2-x)}{R_2} & \frac{(y_2-y)}{R_2} & \frac{(z_2-z)}{R_2} & -1 \\ \frac{(x_3-x)}{R_3} & \frac{(y_3-y)}{R_3} & \frac{(z_3-z)}{R_3} & -1 \\ \frac{(x_4-x)}{R_4} & \frac{(y_4-y)}{R_4} & \frac{(z_4-z)}{R_4} & -1 \end{bmatrix} \quad (2)$$

$$\mathbf{D} = (\mathbf{P}^T \mathbf{P})^{-1} \quad (3)$$

and

$$PDOP = \sqrt{d_{11} + d_{22} + d_{33}} \quad (4)$$

where x , y and z denote the position of the user, x_i , y_i and z_i denote the position of the i -th CubeSat, R_i denotes the distance between the user and the i -th CubeSat, and d_{ij} denotes the element in the i -th row and j -th column of matrix \mathbf{D} . The smaller the $PDOP$ is, the better the configuration is for positioning. As $PDOP$ depends on the configuration of the CubeSats, the z -amplitude (A_z) of the halo orbit and the difference of the phase angles ($\Delta\phi$) of two neighboring CubeSats is used to specify the configuration. Fig. 4 shows different configurations and the corresponding $PDOP$. $PDOP$ can be outrageously high when the CubeSats form a singular geometry with respect to the moon. Fig. 4 only displays the $PDOP$ variation for $PDOP < 50$. Without doubt, the best configuration is that they are distributed evenly throughout the halo orbit. As indicated in the first two panels, $PDOP$ for $\Delta\phi = 90$ deg. is averagely smaller than that for $\Delta\phi = 60$ deg. Furthermore, as A_z is increased to 77,000 km, $PDOP$ exhibits a significant downgrade.

As the configuration with CubeSats evenly distributed along a small halo orbit leads to small $PDOP$, such a configuration

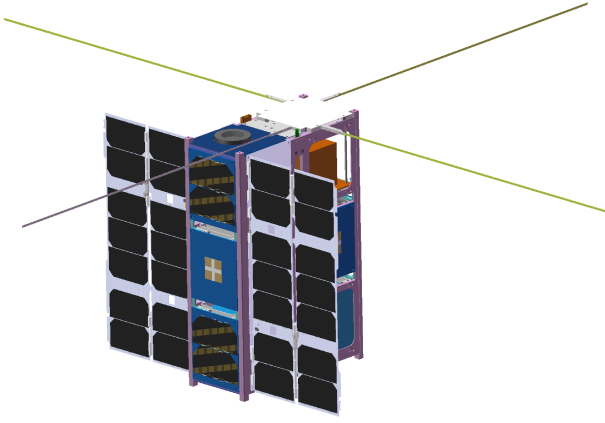


Fig. 3. The CubeSat.

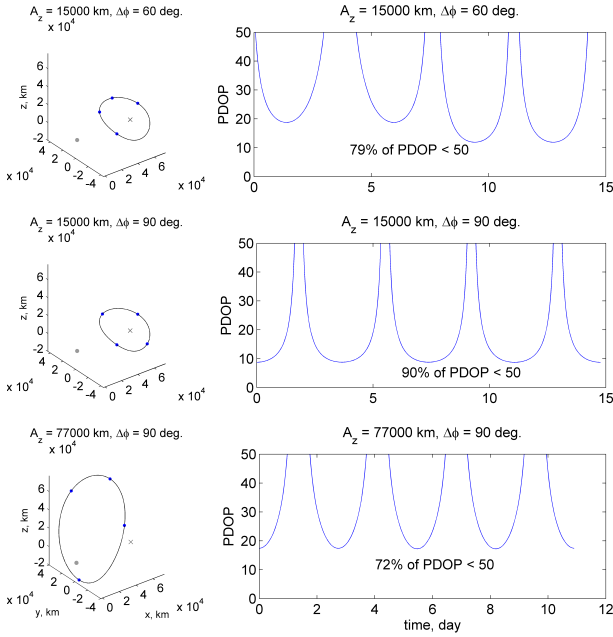


Fig. 4. GODP for different configurations.

with $A_z = 15,000$ km is taken to evaluate the positioning accuracy by simulation. The pseudo-range between the user and the i -th CubeSat, ρ_i , is expressed as,

$$\rho_i = \sqrt{(x - x_i)^2 + (y - y_i)^2 + (z - z_i)^2} + c\Delta t_c \quad (5)$$

where c denotes the speed of light and Δt_c denotes the clock error of the user. The user's coordinates and clock error can be solved by using four pseudo-ranges.¹⁰⁾ With no influence of atmosphere on the Moon, $\Delta\rho_i$ is considered mainly due to the uncertainty of the orbit determination of the i -th CubeSats. According to the operation result of ARTEMIS,¹¹⁾ the initial 3σ of ΔR_C of the orbit determination of a lunar spacecraft is 1 km. The best is 20 m, which is achieved by processing a 10-day batch tracking data. Using a Kalman filter and recursive smoother method, a 3σ of ΔR_C of 185 m can be provided across station-keeping maneuver events. Accordingly, three Monte Carlo tests are performed under three conditions of ΔR_C with 3σ of 1 km, 200 m and 20 m, respectively. To be specific, at every observation instance, 100 randomly-generated error samples are added to the true positions of the CubeSats. The average ΔR of the positioning simulation is shown in Fig. 5. Only the parts average $\Delta R < 5$ km are displayed. It can be seen that

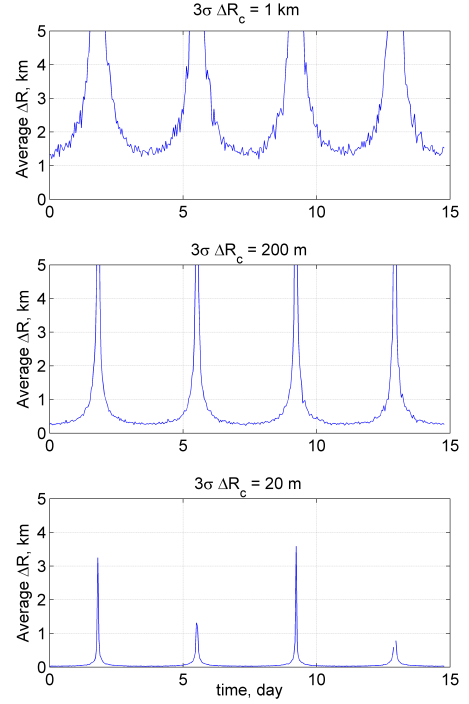


Fig. 5. Average position error of the user under different levels of position uncertainty of the CubeSats

the variation of ΔR follows the that of $PDOP$. The smallest average ΔR are 1.4 km, 260 m and 26 m for the three simulation conditions respectively. Supposing the ΔR_C is 200 m and a ΔR of 3 km is wanted, a working interval lasts 3.4 days, and a blackout interval lasts 4.3 hours. As the period of a low lunar orbit is around 2 hours and the duration of landing is around 12 min, the time waiting to perform landing is not longer than 6.3 hours.

3.2. Lunar Surface Coverage

On the other hand, the accuracy revealed in the previous subsection does not apply to anywhere on the far side of the lunar surface. As real-time positioning require at least four simultaneous pseudo-ranges, the area that can be positioned is the area four CubeSats can be observed simultaneously. Due to the orbital movement of the CubeSats and the curvity of lunar surface, in some areas all four CubeSats cannot be observed at any time or cannot be simultaneously observed all the time. The coverage of the lunar surface by four CubeSats deployed evenly along the halo orbits of different A_z is shown in Fig. 6. It can be seen that, a small halo orbit has a broader converge than a large halo orbit. The far-side area with the longitude within [E125, W125] deg. and latitude within [N75, S75] deg. can be positioned by CubeSats in the halo orbit with $A_z = 15,000$ km. The halo orbit with $A_z = 77,000$ km is a NRHO. While an NRHO has good coverage over the polar region of the moon, the simultaneous coverage in an NRHO turns out to be unsatisfactory in both polar and mid-latitude areas.

4. Low- Δv Trajectory Design

4.1. Station Keeping

Based on the analysis of the positioning performance, a small halo orbit with $A_z = 15,000$ km is chosen for the mission orbit. The station-keeping strategy is to place a Δv at every x - z plane

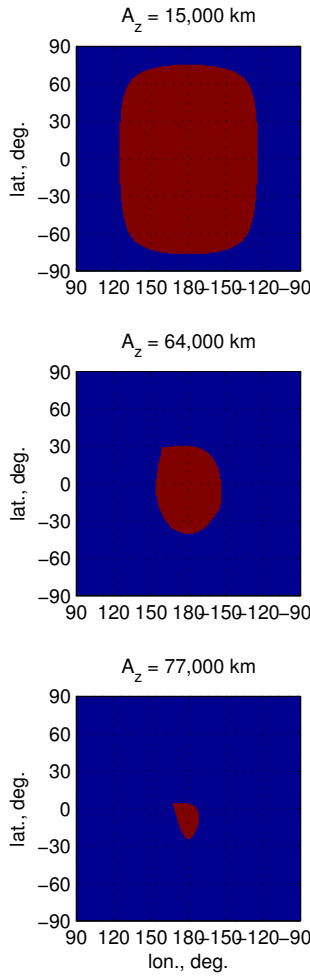


Fig. 6. The coverage (red) of the far side of lunar surface.

crossing such that the x - and z - components of the velocity, v_x and v_z , at the next x - z plane crossing are zero in the high-fidelity model.¹²⁾ Therefore, the maneuver is performed roughly every half period of the initial halo orbit. The high-fidelity model take into account the ephemeris of the Sun, Earth and moon, the harmonic gravitational potential of the Earth and moon up to 8×8 degrees, and solar radiation pressure. In addition, the orbital determination (OD) uncertainty is assumed to be 100 m in position and 0.1 cm/s in velocity. Monte Carlo simulation is performed with the OD uncertainty. The average of the total Δv for a year is 1.8 m/. An example of the orbit maintained by the periodic station keeping Δv is shown in Fig. 7.

4.2. Deployment Trajectories for the Halo Orbit Constellation

It is desirable to deploy four CubeSats along the halo orbit, but it is not economical to launch four CubeSats separately. Therefore, it is assumed that a mother spacecraft carries a lunar lander and four CubeSats to the Moon. In the transfer phase from the Earth to the halo orbit, the rocket and mother spacecraft can provide the required powerful boosts. However, it is infeasible for the mother spacecraft to bring four CubeSats to their different destinations one by one, as the fuel cost will be outrageously high. Therefore, it is assumed that the CubeSats as a whole are released at a stable manifold trajectory heading for the halo orbit at once. Then, the CubeSats are distributed into different phase angles of the halo orbit using on-board

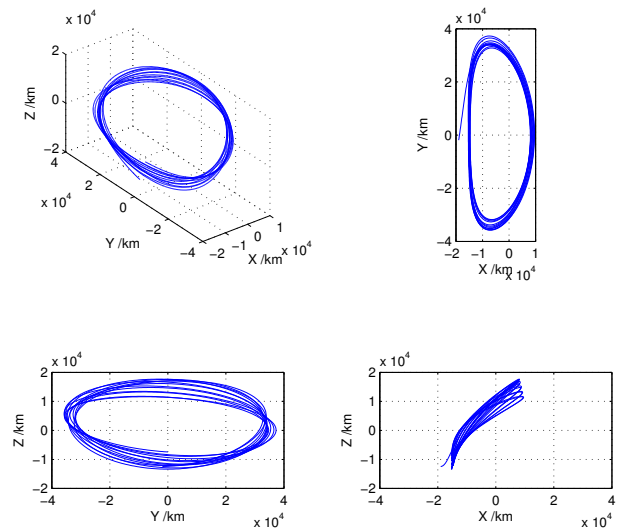


Fig. 7. Station keeping of the halo orbit

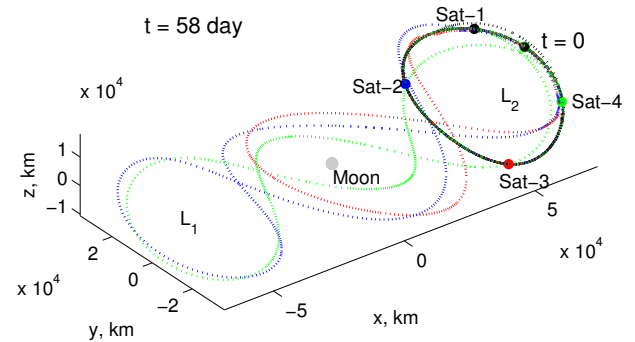


Fig. 8. Phasing trajectories (dashed) to deploy four CubeSats evenly along the halo orbit (solid black).

propulsion systems. Constrained by size, CubeSats have limited propulsion capacity. Therefore, it is needed to design the deployment trajectories that require affordable Δv .

The trajectory design is performed in the CR3BP. Three trajectory design approaches, namely, two-impulse correction manifold, patched manifolds and combination of manifolds and symmetric connecting trajectories have been investigated.¹³⁾¹⁴⁾ Optimal two-impulse trajectories are solved with the MATLAB optimization routine Fmincon. It is found that the contamination of manifolds and symmetric connecting trajectories can lead to various phase angle differences with relatively low Δv . Four CubeSats are distributed evenly along the halo orbit by employing a Δv of 55, 99, 101, 42 m/s, respectively. Fig. 8 shows the deployment trajectories. As demonstrated, three types of trajectories, namely, around the halo orbit, touring the moon, and touring the Earth-moon L_1 point, are involved in the deployment. Starting from the same point in the halo orbit at time $t = 0$, the four CubeSats are distributed evenly along the halo orbit in 58 days.

Although the CR3BP is a simplified model without considering the eccentricity of moons orbit and other perturbations such as solar radiation pressure (SRP). Conclusions and trajectories found in this model are considered to hold roughly true in the reality. However, correction Δv are necessary in high-fidelity models and real operations to deal with those perturbations.

5. Propulsion Systems

5.1. Cold-gas and chemical propulsion systems

As the deployment trajectory require a Δv of 101 m/s and the station keeping control require a Δv of 1.8 m/s per year, it is necessary to find propulsion systems that can meet the Δv requirement. Several propulsion systems are surveyed. A cold-gas propulsion system for CubeSats with a mass of 3.5 kg (estimated propellant mass around 1.93 kg), a volume of 2U, and a propellant Isp of 40 can provide a total impulse of 750 N-sec.* The Δv budget for the CubeSat with a dry mass of 4.8 kg is 104 m/s, which is at the bottom line of the Δv requirement considering that the 2nd and 3rd CubeSats that will use 99 and 101 m/s for deployment. There will be not much Δv budget left for long-term station keeping. However, considering that a landing process only takes 12 min and the preparation a few days, the constellation can hold for a sufficiently long time to support the landing. After that the 2nd and 3rd CubeSats are allowed to escape from the halo orbit. The staying two CubeSats with a remaining budget of 50 m/s can be kept in the halo orbit to provide near-real-time tracking service for the lander whose roving speed is very slow. In that case, the LiAISON tracking technique can be applied.^(6,7) In addition, an 1U chemical propulsion system for CubeSats can provide a total impulse of 1808 N-sec.† The corresponding Δv budget is 250 m/s, which is far sufficient for both deployment and station keeping for a couple of years. On the other hand, chemical propulsion systems risk explosive accidents.

5.2. Electric propulsion systems

As mass and volume are very restricted for CubeSats, the quantity of propellant is also restricted. The electric low-thrust propulsion systems with high specific impulse (Isp) are worth investigating. However, the low thrust may not be able to effectively alter the trajectory within a required period. For instance, the two-impulse deployment trajectory of the 3rd CubeSat that consumes a Δv of 101 m/s during 34 days sets a strict requirement. The following sections address the computation of the optimal continuous-thrust trajectories and shows the relationship between thrust magnitude and required Δv , which serves as a reference for the selection of propulsion systems.

5.2.1. Optimal continuous-thrust trajectories

The equations of motion are expressed by

$$\begin{aligned} \dot{\mathbf{r}} &= \mathbf{v} \\ \dot{\mathbf{v}} &= \mathbf{g}(\mathbf{r}) + \mathbf{h}(\mathbf{v}) + \mathbf{a} \end{aligned} \quad (6)$$

The equations of the co-state of the optimal trajectory should satisfy,

$$\begin{aligned} \dot{\lambda}_{\mathbf{r}} &= -\mathbf{G}^T \lambda_{\mathbf{v}} \\ \dot{\lambda}_{\mathbf{v}} &= -\lambda_{\mathbf{r}} - \mathbf{H}^T \lambda_{\mathbf{v}} \end{aligned} \quad (7)$$

where

$$\begin{aligned} \mathbf{G} &= \partial \mathbf{g} / \partial \mathbf{r} \\ \mathbf{H} &= \partial \mathbf{h} / \partial \mathbf{v} \end{aligned} \quad (8)$$

The direction of optimal acceleration should satisfy,¹⁵⁾

$$\frac{\mathbf{a}}{\|\mathbf{a}\|} = -\frac{\lambda_{\mathbf{v}}}{\|\lambda_{\mathbf{v}}\|} \quad (9)$$

The routine of computing optimal continuous-thrust trajectories consists of three steps. First, the co-state of the solved two-impulse trajectories at the impulse epochs $\lambda(t_{vi})$ ($i = 1, 2$) is obtained, with which the co-state $\lambda(t_0)$ at the initial epoch is derived. Second, the impulse is replaced by a continuous high-thrust (F) arc. The $\lambda(t_0)$ computed from the 1st step is adjusted to meet the terminal constraint and minimize the Δv . Third, a continuation method is used where the F is decreased step by step, and the optimal trajectory solution for the current F becomes the initial guess for the solution with the next F .

To be specific, in the 1st step, since the impulse direction is known, the direction of $\lambda_{\mathbf{v}}(t_{vi})$ ($i = 1, 2$) is also determined according to Eq. (9). In addition, as the two impulsive Δv are placed at the optimal epochs, $\|\lambda_{\mathbf{v}}(t_{vi})\| = 1$ and $\dot{\lambda}_{\mathbf{v}}(t_{vi}) = 0$ ($i = 1, 2$).¹⁶⁾ Then, $\lambda_{\mathbf{v}}(t_{vi})$ ($i = 1, 2$) is determined. $\dot{\lambda}_{\mathbf{v}}(t_{v1}) = 0$ is assumed to obtain an initial guess for $\lambda_{\mathbf{r}}(t_{v1})$. By applying differential correction, the $\lambda(t_{v1})$ that can lead to $\lambda_{\mathbf{v}}(t_{v2})$ through the integration of Eq. (7) from t_{v1} to t_{v2} is solved. With $\lambda(t_{v1})$ obtained, $\lambda(t_0)$ is computed by backward integrating Eq. (7).

The 2nd step is to solve the finite-thrust trajectory. Given a high F , the magnitude of \mathbf{a} is also specified. (Note that in this analysis where the propulsion specification is not specified, the mass of the CubeSat is assumed constantly 7 kg.) Two variables, the boundary epochs (t_{F1} and t_{F2}) of the 1st thrusting arc corresponding to Δv_1 are involved in this step. The initial guesses for t_{F1} and t_{F2} should be before and after t_{v1} , respectively. The thrusting duration, Δt (i.e. $t_{F2} - t_{F1}$), is approximated by $\Delta v_1/a$. Since the optimal transfer trajectory is symmetric about the x-z plane, the terminal constraint at the mid-epoch, $(t_0 + t_f)/2$, is

$$\begin{bmatrix} y & v_x & v_z & \lambda_{rx} & \lambda_{vx} & \lambda_{vz} \end{bmatrix} = \mathbf{0} \quad (10)$$

The initial guess for $\lambda(t_0)$ is obtained from the 1st step. $\lambda(t_0)$, t_{F1} and t_{F2} are optimized, such that the terminal constraint is met and Δt is minimized. The second half of the trajectory (i.e. the trajectory after the x-z plane crossing) is symmetric to the first half and thus is easily obtained. The solved $\lambda(t_0)$, t_{F1} and t_{F2} become the initial guess for the solution with the next sampled F .

5.2.2. Results

The most critical case, the deployment trajectory of the 3rd CubeSat, is taken for the discussion. Following the computation routine, optimal continuous-thrust trajectories are computed and corresponding the Δv vs F is revealed, which is shown in Fig. 9. Fig. 10 shows the continuous-thrust deployment trajectory with a thrust of 1 mN, which consumes a total Δv of 114 m/s. As seen in Fig. 9, no solution exists for the situation with a thrust smaller than 0.3 mN. There are several electric propulsion systems with a thrust greater than 0.3 mN (see surveys of propulsion systems for interplanetary and lunar CubeSats by Tardivel et al.¹⁷⁾ and Stibbard et al.¹⁸⁾). The Δv vs F result can serve as a reference for propulsion system sizing (concerning F , Isp and propellant mass).

* JPL MarCO Micro CubeSat Propulsion System, <http://www.cubesat-propulsion.com/jpl-marco-micro-propulsion-system/>, accessed October 2 2016.

† VACCO Green Mono Prop System, <http://www.cubesat-propulsion.com/wp-content/uploads/2015/10/adn-micropropulsion-system.pdf>, accessed October 2 2016.

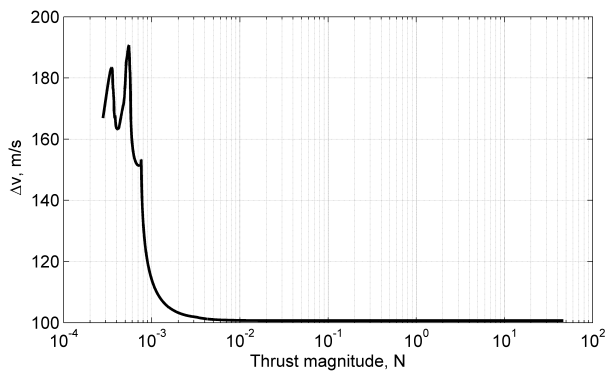


Fig. 9. Δv vs thrust magnitude for optimal continuous-thrust trajectories.

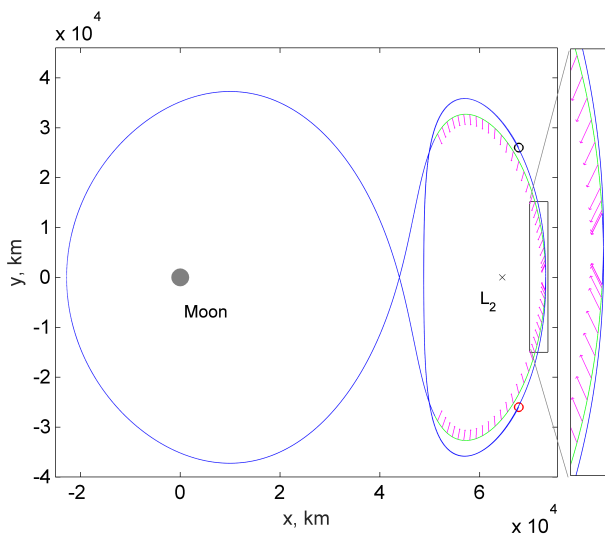


Fig. 10. Continuous-thrust deployment trajectory with a thrust magnitude of 1 mN.

6. Conclusion

This paper presents the mission design and analysis of a CubeSat mission for positioning users on the far side of the moon. The analysis reveals that small halo orbits with A_z around 15,000 km are favorable with relatively good coverage of the lunar surface and geometry for positioning. The best achievable positioning accuracy is 80 m. In addition, for a desirable positioning accuracy of 3 km, a working period lasts 3.4 days and a waiting period lasts 4 to 6 hours. As it is required to deploy four CubeSats evenly along the halo orbit and keep them in the halo orbit, deployment trajectories and station-keeping control were designed. It is obtained that a Δv around 100 m/s is needed for deployment, and a Δv of 1.8 m/s is needed for the station keeping in a year. Applicable propulsion systems are discussed with the result of Δv vs thrust magnitude, which is computed with a continuous-thrust trajectory optimization routine. Several modern propulsion systems for CubeSats are found applicable. While the present work is intended for the proposed lunar-far side positioning mission, the analysis approaches and results are extensible to other interplanetary CubeSat missions, which will play an important role in future space exploration.

Acknowledgments

This work is supported by the Advanced Study Program (grant CSU-QZKT-201711) of Technology and Engineering Center for Space Utilization, Chinese Academy of Sciences, and National Natural Science Foundation of China (NSFC) (grant 11372311). The authors acknowledge Yang Gao and Wenbin Wang for their advice and comments. Lei Liu acknowledges the support by China Postdoctoral Science Foundation (grant 2016M592947) and NSFC (grant 11303001 and 61573049).

References

- 1) A. T. Klesh, INSPIRE AND MARCO - TECHNOLOGY DEVELOPMENT FOR THE FIRST DEEP SPACE CUBESATS, in: 41st COSPAR Scientific Assembly, Turkey.
- 2) M. Kuppers, I. Carnelli, A. Galvez, K. Mellab, P. Michel, the AIM team, The Asteroid Impact Mission (AIM), in: European Planetary Science Congress 2015, Vol. 10, 2015.
- 3) Space Launch Systems (SLS) Secondary Payload User's Guide, Tech. rep., NASA (2015).
- 4) J. O. Burns, D. A. Kring, J. B. Hopkins, S. Norris, T. J. W. Lazio, J. Kasper, A lunar L2-Farside exploration and science mission concept with the Orion Multi-Purpose Crew Vehicle and a teleoperated lander / rover, *Advances in Space Research* 52 (2) (2013) 306–320. doi:10.1016/j.asr.2012.11.016.
- 5) F. Li, H. Zhange, X. Wu, J. Ma, W. Zhou, THE SCIENTIFIC VALUE AND TECHNICAL CHALLENGE OF CHANG'E-4 LANDING ON THE FAR-SIDE OF THE MOON, in: 41st COSPAR Scientific Assembly, Turkey.
- 6) K. Hill, G. H. Born, Autonomous Interplanetary Orbit Determination Using Satellite-to-Satellite Tracking, *Journal of Guidance, Control, and Dynamics* 30 (3) (2007) 679–686. doi:10.2514/1.24574.
- 7) S. G. Hesar, J. S. Parker, J. M. Leonard, R. M. Mcgrnaghan, G. H. Born, Lunar far side surface navigation using Linked Autonomous Interplanetary Satellite Orbit Navigation (LiAISON), *Acta Astronautica* 117 (2015) 116–129. doi:10.1016/j.actaastro.2015.07.027.
- 8) K. C. Howell, Three-Dimensional, Periodic, 'Halo' Orbits, *Celestial Mechanics* 32 (1) (1984) 53–71.
- 9) E. J. Doedel, R. C. Paffenroth, H. B. Keller, D. J. Dichmann, J. Galán-Vioque, A. Vanderbauwhede, Computation of Periodic Solutions of Conservative Systems with Application to the 3-Body Problem, *International Journal of Bifurcation and Chaos* 13 (06) (2003) 1353–1381. doi:10.1142/S0218127403007291.
- 10) D. A. Vallado, *Fundamentals of Astrodynamics and Applications*, Microcosm Press and Springer, 2007.
- 11) M. Woodard, D. Cosgrove, P. Morinelli, J. Marchese, B. Owens, D. Folta, Orbit determination of spacecraft in Earth-Moon L1 and L2 libration point orbits, *Advances in the Astronautical Sciences* 142 (1) (2012) 1683–1696.
- 12) L. Liu, J.-f. Cao, Design and Stationkeeping of Lissajous trajectories about the Earth-Moon collinear libration points, in: *Proceedings of IEEE Chinese Guidance, Navigation and Control Conference*, Yantai, China.
- 13) H. Chen, Y. Meng, J. Ma, Phasing Trajectories for a CubeSat Lunar Far-side Positioning Mission, in: *Workshop on JAXA Astrodynamics and Flight Mechanics*, Sagamihara, Japan, 2016.
- 14) H. Chen, J. Ma, Phasing Trajectories to Deploy a Constellation in a Halo Orbit, *Journal of Guidance Control, and Dynamics*-doi:10.2514/1.G002518.
- 15) D. F. Lawden, *Optimal Trajectories for Space Navigation*, Butterworths, 1963.
- 16) D. J. JEZEWSKI, H. L. ROZENDAAL, An efficient method for calculating optimal free-space n-impulse trajectories., *AIAA Journal* 6 (11) (1968) 2160–2165. doi:10.2514/3.4949. URL <http://arc.aiaa.org/doi/10.2514/3.4949>
- 17) S. Tardivel, S. Campagnola, N. Ozaki, A. T. Klesh, Interplanetary

Nanospacecraft Travel Capabilities, 26th AAS/AIAA Space Flight Mechanics Meeting (2016) 1–5.

18) M. Stibbard, S. Tuttle, Current Attainability of a Lunar Microsatel-

lite Mission for Universities and Similar, in: 30th International Space technology and sciences, Kobe, Japan, 2015.